Chapter 20

Bright-Field Imaging and Optical Coherence Tomography of the Mouse Posterior Eye

Mark P. Krebs, Mei Xiao, Keith Sheppard, Wanda Hicks, and Patsy M. Nishina

Abstract

Noninvasive live imaging has been used extensively for ocular phenotyping in mouse vision research. Bright-field imaging and optical coherence tomography (OCT) are two methods that are particularly useful for assessing the posterior mouse eye (fundus), including the retina, retinal pigment epithelium, and choroid, and are widely applied due to the commercial availability of sophisticated instruments and software. Here, we provide a guide to using these approaches with an emphasis on post-acquisition image processing using Fiji, a bundled version of the Java-based public domain software ImageJ. A bright-field fundus imaging protocol is described for acquisition of multi-frame videos, followed by image registration to reduce motion artifacts, averaging to reduce noise, shading correction to compensate for uneven illumination, filtering to improve image detail, and rotation to adjust orientation. An OCT imaging protocol is described for acquiring replicate volume scans, with subsequent registration and averaging to yield three-dimensional datasets that show reduced motion artifacts and enhanced detail. The Fiji algorithms used in these protocols are designed for batch processing and are freely available. The image acquisition and processing approaches described here may facilitate quantitative phenotyping of the mouse eye in drug discovery, mutagenesis screening, and the functional cataloging of mouse genes by individual laboratories and large-scale projects, such as the Knockout Mouse Phenotyping Project and International Mouse Phenotyping Consortium.

Key words Bright-field fundus imaging, Optical coherence tomography, Noninvasive ocular imaging, Mouse eye phenotyping, Mouse vision research

1 Introduction

Since it was first described in the 1990s [1–3], noninvasive imaging of the posterior mouse eye (fundus) has been a mainstay of genetic discovery and hypothesis testing in mouse vision research. This region of the eye includes the retina, retinal pigment epithelium (RPE), and choroid, in which pathological changes occur in many blinding diseases. In contrast to indirect ophthalmoscopy [1, 4], which can be used by a highly skilled observer to identify phenotypic differences rapidly, noninvasive imaging techniques

Gabriele Proetzel and Michael V. Wiles (eds.), *Mouse Models for Drug Discovery: Methods and Protocols*,
Methods in Molecular Biology, vol. 1438, DOI 10.1007/978-1-4939-3661-8_20,

provide an objective permanent record that may be scrutinized more thoroughly and is amenable to quantitative analysis. Noninvasive imaging techniques also facilitate repeated examination at different times, allowing short-term assessment of ocular properties, such as blood flow in the retinal vasculature, and long-term studies, for example longitudinal analysis of ocular development or disease progression in individual mice as they age. The most widely used methods for imaging the posterior eye in live mice parallel those of the human ophthalmology clinic: bright-field or fluorescence fundus imaging, also known as fundus photography [1, 4]; scanning laser ophthalmoscopy [5, 6]; and optical coherence tomography (OCT) [7, 8].

In this chapter, we present our approach to two of these methods, bright-field fundus imaging and OCT. Other recent articles provide alternative protocols for these and related approaches [4, 9]. The protocols, which are presented in detail below, can be summarized briefly as follows: the eyes of mice are dilated and the animals are held (bright-field fundus imaging) or anesthetized and restrained (OCT) on a support stand that can be translated or rotated in up to three dimensions (Fig. 1). The positions of the mouse and/or instrument light path are then adjusted so that the ocular region of interest is optimally oriented, illuminated, and focused. Multi-frame videos (bright-field fundus imaging) or replicate volume scans (OCT) can then be acquired. Finally, the scans are saved in or converted to *.tif format, registered, averaged, and processed digitally to enhance image detail and minimize artifacts.

In bright-field fundus imaging, the pupil is dilated and a specialized microscope is aimed into the mouse eye to provide illumination and imaging capability. In earlier work, researchers used a clinical fundus camera adapted for the mouse eye with an intervening adaptor lens [1–4], and results obtained by this approach continue to be published. However, over the past decade, new ocular imaging systems have become available that are designed for use with a contact liquid or gel between the microscope objective and the mouse corneal surface. These microscopes employ a carefully developed optical system that shines light into the eye and collects the reflected image on a color sensor. The digital signal is acquired in video mode and can be further processed by the manufacturer's software or exported for analysis by other programs that may offer additional functionalities.

The fundamental principle underlying OCT is that light passes at differing rates through the translucent compartments and tissue layers of the eye, which differ in refractive index. In spectral domain OCT, the technology available in most commercial OCT instruments, a near-infrared narrow bandwidth beam is aimed into the dilated eye (typically without an intervening contact liquid) and simultaneously split to a reference mirror. The beam reflected from

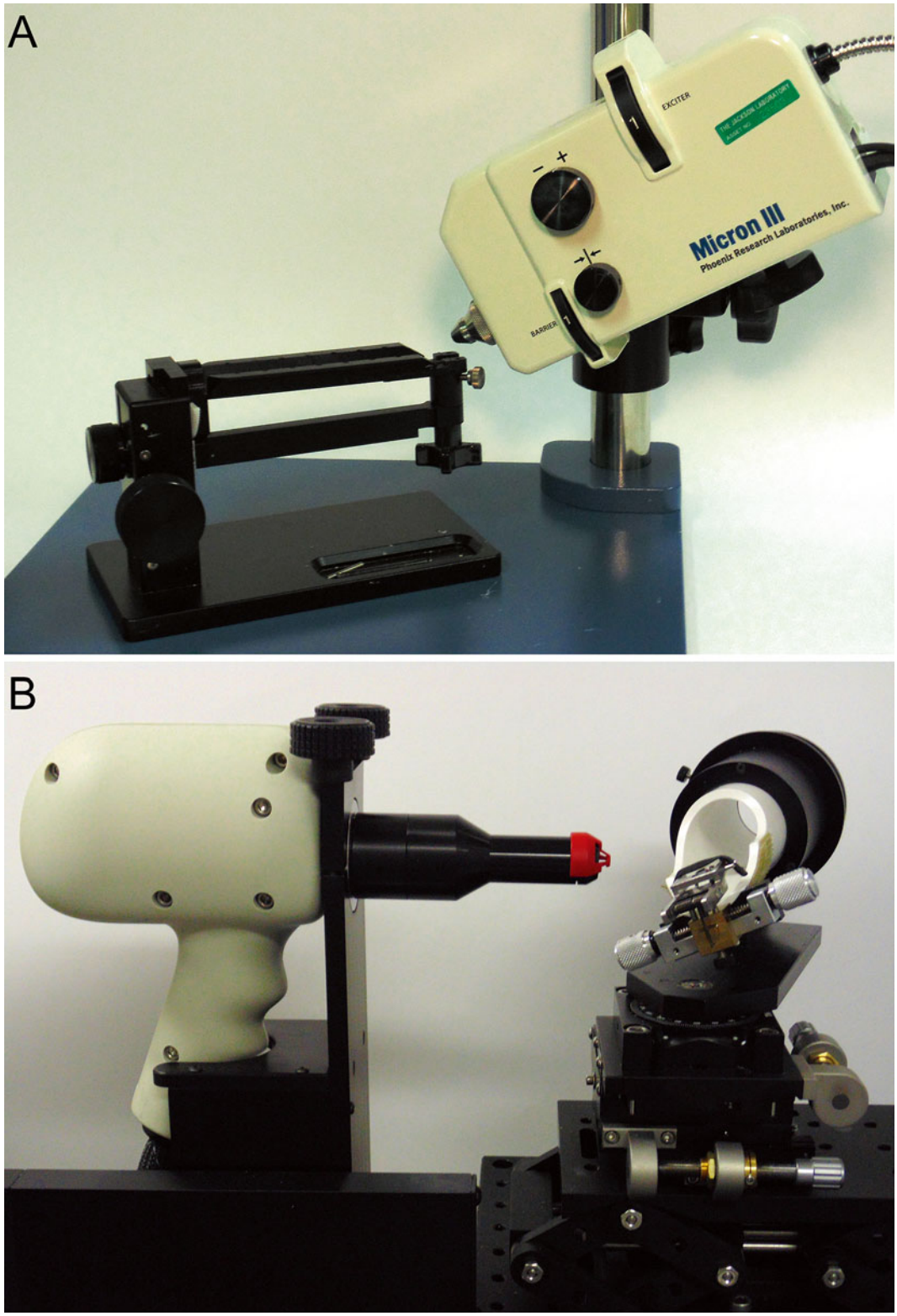

Fig. 1 Noninvasive imaging mouse platforms. (**a**) Camera and stand of a Phoenix Research Laboratories instrument. The Micron III system is shown; the camera and stand of the Micron IV system are very similar. (**b**) Probe and stand of a Bioptigen ultrahigh-resolution (UHR) Envisu R2210 spectral domain OCT (SDOCT) imaging system

the eye interferes with the reference beam, and the resulting spectral domain interference pattern is transformed mathematically into a plot of tissue reflectivity by axial distance (A-scan). The beam is swept in a radial plane to produce the equivalent of a histological cross section (B-scan), and in some instruments can also be advanced in raster fashion to create a dataset (rectangular volume) that captures the three-dimensional structure of ocular tissue. Commercial instruments that offer rapid acquisition rates over large capture areas are among the most widely used by mouse vision researchers. These systems provide software for image processing and analysis, but also allow export of the data in a format compatible for analysis with other programs.

A key aspect of our approach is the use of post-acquisition processing to improve image quality. Ideally, images would be obtained with high signal-to-noise in a single exposure that is short enough to freeze motion artifacts, which arise from eye movement, heartbeat, respiration, and mouse movement. However, as currently available commercial instruments yield relatively noisy data in a single short exposure, image quality can be improved by acquiring multiple exposures, followed by registration (image alignment) and averaging. Digital processing is used further to improve image appearance and ensure uniformity for downstream applications by adjusting orientation, compensating for uneven illumination, sharpening, and optimizing brightness and contrast. For this purpose, we have developed a plug-in and macro that make use of the public domain Java-based software ImageJ [10] (currently released as ImageJ2 [11]), which is bundled with many useful plug-ins in a distributed version of ImageJ named Fiji [11, 12]. Processed images are suitable for downstream analysis, including introduction into automated pipelines for digital survey and statistical image comparison. Our processing tools are available through links provided in this chapter.

The bright-field and OCT imaging methods described here have been used in experiments documenting new mouse lines, including a C57BL/6N-derived strain bearing a targeted correction of the *Crb1*^{rd8} mutation [13] and several new models of human disease [14–17] identified through the Translational Vision Research Models (TVRM) program [18, 19] at The Jackson Laboratory (JAX). In addition, the bright-field fundus imaging approach has been adopted by the Knockout Mouse Phenotyping Project (KOMP^2) pipeline at JAX. The methods aim toward the high-quality end of the quality-quantity continuum, which contrasts the need for data with high information content against the need for examining large numbers of subjects. These considerations are particularly important for large-scale projects that require high throughput, including mutagenesis screens, drug discovery programs, big data analysis, and gene cataloging initiatives, such as

KOMP² and the International Mouse Phenotyping Consortium (IMPC; http://www.mousephenotype.org). While the methods presented here may have suboptimal throughput for certain large-scale projects, they may be easily accelerated if lower image quality is acceptable.

2 Materials

Mice: Desired mouse strain, pigmented or albino, bred and maintained with institutional approval (for example, the ARVO Statement for the Use of Animals in Ophthalmic and Vision Research).

Anesthetic cocktail: 1.6 mL Ketamine (100 mg/mL), 1.6 mL xylazine (20 mg/mL), and 6.8 mL sodium chloride (0.9% w/v).

Dilating agent: 1% Atropine.

Contact gel: GenTeal Severe Dry Eye Relief, Lubricant Eye Gel, or Goniovisc Eye Lubricant.

Corneal hydration agent: Systane Ultra Lubricant Eye Drops.

Ocular imaging system: Micron III or IV (Phoenix Research laboratories), Envisu R2210 (Bioptigen), or equivalent imaging systems.

Surgical spears: Sugi, Kettenbach, USA.

Computer: Personal computer (Mac OS X or Windows based) with good graphics capability, 64 bit.

Software: Fiji can be downloaded and installed from http://fiji.sc/Fiji. Once installed, we suggest accepting all updates available except for developer tools, which are not needed for the protocols described here. Plug-ins are necessary and need to be installed to provide for registration of color images [20]. This is done by dragging the Image_Stabilizer.class and Image_Stabilizer_Log_Applier.class files onto the Fiji menu bar.

3 Methods

3.1 Bright-Field Fundus Image Acquisition and Processing

These instructions are based on the use of a Micron IV imaging system (Phoenix Research Laboratories, Pleasanton, CA), using Streampix (NorPix, Montreal, Quebec, Canada) as the video acquisition interface. The instructions also apply to the Micron III imaging system and to the use of Discover (Phoenix Research Laboratories) as the video acquisition software in newer installations, with exceptions noted.

1. Set Streampix so that video files are stored automatically as a *.tiff image stack immediately following acquisition (*see* **Note 1**). Under *Streampix Settings* > *Recording* > *When a recording ends* > *Auto export sequence to*, select TIFF image files. Under … > *General*, select *Save images as TIFF image files.* Under … > *Limits*, select *Limit sequence on disk to X frames* and set frames to the desired number, typically 100. Also set *Loop recording when limit is reached* to *No.* Finally, under *More…* > *Images*, set *TIFF format* to *Multi-TIFF* (*see* **Note 2**).
2. Adjust the Streampix software so that each video file automatically receives a timestamp and datestamp: under *Streampix Settings* > *Auto Naming* > *Auto-naming for EXPORTING to image files*, check the box labeled *Scheme* and complete the default entry in the adjacent box so that it reads (*workingfolder*)\(*customtoken*) (*date*)_(*time*). This ensures that every image video will have a unique name, and that the date and time of each acquisition file will be associated with the file, independently of when it is moved or copied (*see* **Note 3**).
3. Set up the acquisition session by creating a new folder and browsing to select it under *Streampix Settings* > *Workspace(s)* > *Default Working Folder*. As a simple organizational aid, include the acquisition date (in *yymmdd* format) at the beginning of the folder name.
4. Create a unique sample identifier for your first sample by entering it under *Autonaming* > *Default value of the (customtoken)*; this will be updated manually with each additional sample, or automatically if you elect to increment the *customtoken* automatically according to *Edit (increment) token settings.* For recordkeeping, use a unique sample identifier that includes the strain, mouse number, and eye designation, such as *JR0664 1528 OS.*
5. Turn on the lamp. Wave in front of the lens to ensure that all parts of the system are functioning properly; an image of your moving hand should appear on the live display.
6. Set the color balance of the imaging sensor at first use and every few months thereafter. Hold a white card in front of the lens, move the card so that each color channel falls within the 0–255 intensity range on the imaging histogram display, and click on the automatic white balance (AWB) button in the imaging dialog box (*see* **Note 4**). The correction will be completed within a few seconds.
7. Dilate the pupils of mice to be examined. Restrain the mouse firmly in one hand and squeeze a drop of dilating agent directly onto the surface of both eyes (or one, if only one will be examined). Allow 5–10 min for dilation to occur; pupils will remain dilated for several hours when atropine is used. Whiskers

(vibrissae) may be trimmed to prevent them from interfering with imaging, but with practice they may be displaced by the camera nosepiece, so trimming becomes unnecessary (*see* **Note 5**).

8. Scruff the mouse (Fig. 2a) and place a generous drop of contact gel on the eye to be imaged (*see* **Note 6**).
9. Place the mouse on the imaging stand (Fig. 2b). To allow the camera nosepiece to approach without hitting the stand, the eye should be approximately centered on the groove perpendicular to the long axis of the stand (Fig. 2b).
10. Image the head and/or eye position to permit downstream adjustment of ocular rotation. Adjust the camera gain to a setting of 12 and turn the illumination control to its maximum value. To image the head, move the camera forward with the lateral positioner until the head including the eye and nose fill the image frame. Adjust the focus and the illumination intensity to minimize overexposed regions and acquire a snapshot. To image the external eye, move the camera forward with the midline axial knob until the eye and tear duct fill the image frame (Fig. 2c). Make sure that the pupil and the ventral edge of the nictitating membrane (third eyelid) are clearly defined and free of reflections, as these features will be used to measure ocular rotation. Adjust focus and illumination and acquire a snapshot (*see* **Note 7**).
11. Set the exposure time to a minimum. An upgrade to the Streampix software available through Phoenix Research Laboratories allows the user to adjust the exposure time in the *JAI GigE Control* panel, which shows camera settings. Typically, a value of 20 ms is used (*see* **Note 8**).
12. Reset the gain to 0 to ensure the best signal-to-noise ratio.
13. Adjust the mouse position so that the eye is centered on the pupil. Carefully move the camera forward until the retina is visible. Initially adjust the focus on the superficial vasculature (large blood vessels on the retinal surface), which are typically the easiest landmarks to detect.
14. Carefully adjust the mouse position so that the optic nerve head (ONH) is centered on the displayed image and aligned with the optical axis of the camera. The superficial vessels radiating from the ONH resemble spokes on a bicycle wheel with the ONH being the axle. Use the vertical position knob on the mouse stand to move the displayed image of the ONH up or down, coordinately adjusting the tilt knob to keep the ONH axle free of tilt. If needed, move or rotate the base of the stand to center the ONH laterally. The image center can be seen as a dim spot on the displayed image (*see* **Note 9**).

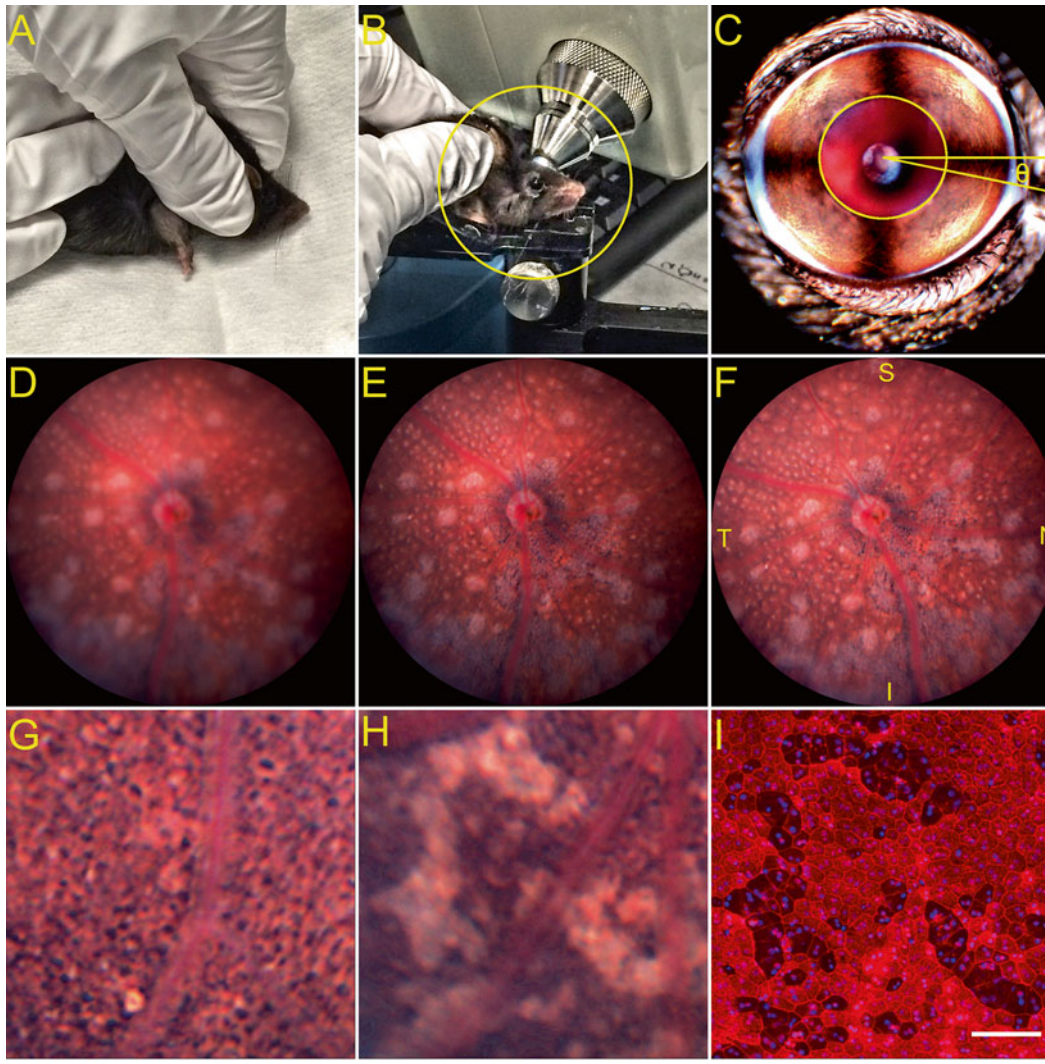

Fig. 2 Bright-field fundus imaging. (**a**) Manual restraint (scruffing) of unanesthetized mice for imaging showing position of right thumb between the mouse ear and front leg. (**b**) Positioning of mouse on the stand for imaging. In this case, the left eye is being imaged and the top of the stand has been swiveled accordingly. Contrast within the area inside the *circle* has been enhanced in Fiji to visualize the mouse. (**c**) External view of a dilated right mouse eye obtained with the Micron IV camera. The superimposed diagram shows an ellipse outlining the pupil (*circle*) and the angle (θ) between horizontal and a line drawn from the center of the ellipse to the ventral edge of the upper nictitating membrane. This angle is applied to bright-field fundus images of the same eye to achieve a uniform orientation. (**d**) Single frame from an unprocessed video acquisition of 100 frames. The right eye of a mouse identified in a chemical mutagenesis screen as part of the TVRM program was imaged. (**e**) Same image as in (**d**) after registration and averaging with *ImageStabilizeMicronStack*. (**f**) Same image as in (**d**) after adjusting orientation using *Image*>*Transform*>*Rotate* with an angle of −11.0° determined as in **step 26**, and with *Bilinear* interpolation, and by correcting for nonuniform illumination using *Polynomial Shading Corrector* with *Degree x* and *Degree y* set to 10 and *Regularization percent of peak* set to 60. The image was also adjusted with *Image*>*Adjust*>*Brightness*/*Contrast*. Retinal quadrants are indicated as *S* superior, *N* nasal, *I* inferior, and *T* temporal. (**g**) Detection of the RPE polygonal lattice in processed images (Micron III) of a mutant strain that exhibits retinal degeneration in the form of photoreceptor loss. (**h**) Apparent loss of pigment from RPE cells in processed images (Micron III) of the eye of a mutant strain (*tvrm267*) that shows RPE defects [15]. (**i**) Fluorescence microscopy of an RPE flat mount stained to reveal filamentous actin (rhodamine phalloidin, *red*) and nuclei (DAPI, *blue*) showing close correspondence of RPE lesions with those observed in processed bright-field fundus images. Scale bar, 100 μm

15. Readjust the focus so that the features of interest are clearly defined. For example, lesions in the RPE are typically in a different focal plane than the superficial retinal vessels.
16. Adjust the illumination so that no channel exceeds a value of ~200 on the histogram of pixel intensity. On the Micron IV, the red channel is usually the most intense.
17. Once the ONH is centered and free of tilt, features of interest are focused, and illumination is optimized, initiate a video acquisition by clicking on *Record* with the computer mouse or stepping on the footswitch, if available. Monitor the display to ensure that no abrupt movements, such as blinks, occur during the recording (if observed, simply click *Stop* to abort the recording). If the data acquisition has been pre-set properly, conversion of the video to TIFF (*.tif on Mac platforms) format should complete within a few seconds immediately after the acquisition finishes.
18. Repeat the process several times until you are satisfied that a high-quality video has been acquired.
19. Repeat with **steps 8–18** for the next eye or mouse to be imaged after updating the sample information as described in **step 4**.
20. Once all data have been collected, prepare the files for processing with *ImageStabilizeMicronStack*. Although the plug-in is designed to identify and process only *.tif stacks containing more than one slice, it may be convenient to prepare the output from the recording session. Move all video files in TIFF format to a single folder, named *Raw*. Remove *.seq files, which can only be read by Streampix, as well as any files that are not of full length, such as recordings that were stopped prematurely. Move snapshots in TIFF format to a folder named *Headshots*; these can be identified and sorted by their relatively small size (~2 MB). Create a third folder named *Processed* to hold the processed data.
21. Launch Fiji and drag the *ImageStabilizeMicronStack* macro onto the menu bar to compile it.
22. Use the *ImageStabilizeMicronStack* macro to register, average, and sharpen all of the videos collected during the session. The macro will prompt the user for input and folders (*Raw* and *Processed*, respectively) (*see* **Note 10**).
23. The *ImageStabilizeMicronStack* macro outputs images that are sharpened by applying two rounds of *Process> Filters> Unsharp Mask…* (compare Fig. 2e, d). The rationale for using a registered and averaged stack as input is that sharpening introduces noise if a single unaveraged frame is used. The justification for two rounds of *Unsharp Mask…* is that this approach appears to

reveal true ocular features, such as the RPE cells shown in Fig. 2g, and yields image details that correspond well with microscopic views of the same tissue (compare Fig. 2h, i). However, if desired, the degree of unsharp masking can be reduced simply by decreasing the *Mask Weight* parameter of the *Unsharp Mask…* command within the *ImageStabilizeMicronStack* macro. A helpful analysis of applying unsharp mask to scientific image data has been presented [21].

24. Curate the processed images to identify and retain one with the highest quality. From the *Processed* folder, select all images with the same *customname* (ignoring the time and date stamps) and drag them onto the Fiji menu bar. Use *Window > Tile* to distribute the images over the screen. Close images that show evidence of poor focus, motional blurring, or bright artifacts associated with eyelashes or bubbles. Identify the highest quality image among those that remain.
25. Delete all images and raw datasets except for those that correspond to the high-quality images selected. This approach assures that a minimal number of raw and processed images are archived (that is, reduces storage space).
26. If uniform orientations are desired, use the external eye snapshots to approximate the orientation angle. Draw a line from the center of the pupil to the ventral edge of the upper nictitating membrane as shown in Fig. 2c. The angle of displacement (θ) of this line from horizontal, which is chosen arbitrarily as an orientation reference, appears in the Fiji menu bar. Rotate the fundus image with *Image > Transform > Rotate* by $\theta°$ (right eye) or $\theta + 180°$ (left eye).
27. Image stacks are a convenient form to store, process, review, and analyze large numbers of bright-field images. Fiji may be used to create image stacks simply by dragging a folder of images onto the menu bar and selecting "create image stack" to the dialog box. Individual images within the stack can be reviewed by moving the scroll bar at the base of the image or by pressing the right or left arrow keys. Operations such as contrast adjustment or masking can be performed on the entire stack. The *Image > Stacks > Make Montage…* operation is particularly useful for creating arrays of images for review or publication (Fig. 3).

3.2 OCT Image Acquisition and Processing

These instructions are based on the use of an ultrahigh resolution (UHR) Envisu R2210 spectral domain OCT (SDOCT) imaging system (Bioptigen, Durham, NC), with InVivoVue 1.4.0.4260 software installed on a 32-bit Windows computer as supplied by the manufacturer. The instructions may be adapted to acquire and process OCT data from other instruments as long as data are

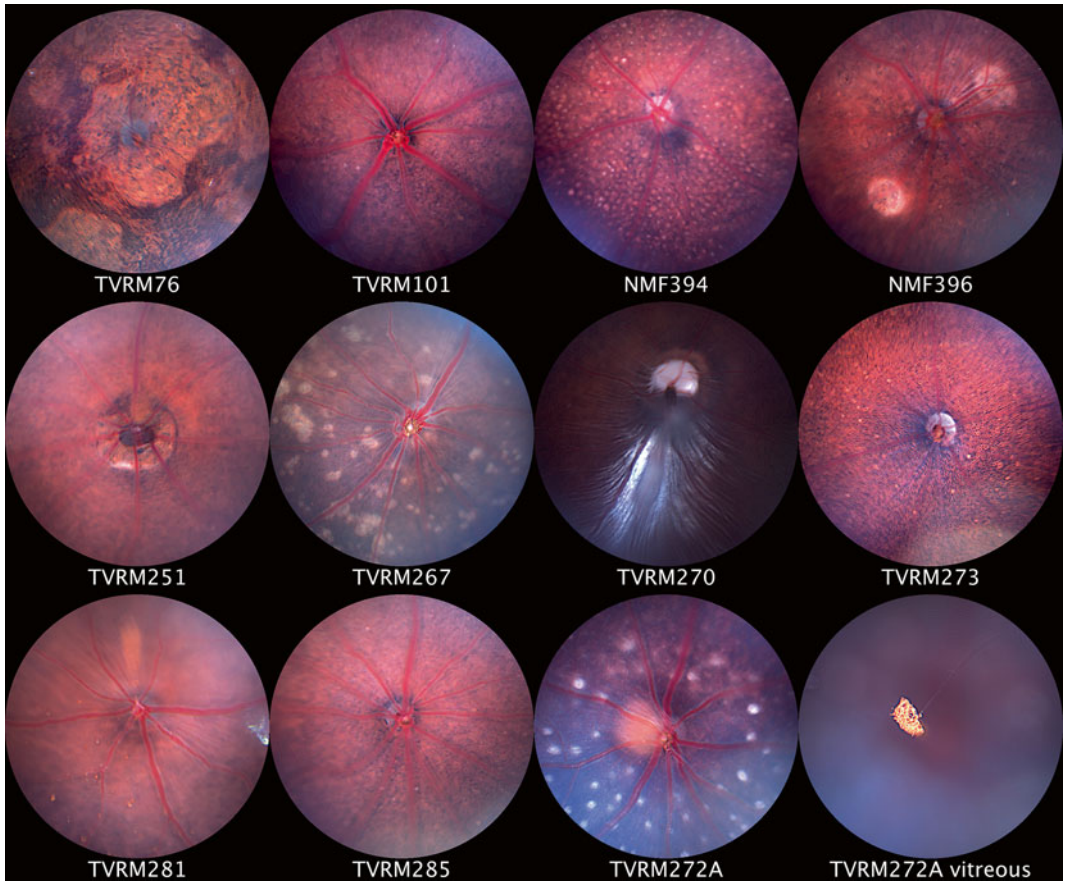

Fig. 3 Montage display of bright-field fundus images obtained with the Micron III imaging system and processed with *ImageStabilizeMicronStack* as described in this protocol, except that no correction was made for uneven image illumination or orientation. Using Fiji operations, processed images were subsequently combined in a stack, adjusted for brightness and contrast, cropped with a circular mask, and displayed in an array. The figure shows the varied phenotypes of mutant and putative mutant mice identified by indirect ophthalmoscopy screens of chemically mutagenized mice for ocular disease phenotypes as part of the TVRM program at JAX [18, 19]

available in *.tif format (required for processing). This capability has been demonstrated with data from an extra-high-resolution (XHR) Envisu R4110 SDOCT with InVivoVue 2.2.20 software on a 64-bit platform (Bioptigen), and the Micron IV imaging system fitted with an OCT accessory (Phoenix Research Laboratories).

1. Turn on the instrument and its light source, and launch the InVivoVue software to prepare for image acquisition. On first use, set up a template to record ten replicate scans for each eye in rectangular volume mode, typically with scans of 1000 A-scans per B-scan × 100 B-scans per rectangular volume × 1 frame (no averaging) over an area of 1.4–1.6 mm. Check the box to designate OD or OS; also uncheck the box labeled

"Save OCU files" to reduce the size of saved data by two-thirds. Replicate scans must be created as a "protocol." Once this protocol has been saved, it is recalled when an exam is initiated (*see* **Note 11**).

2. Enter mouse-specific information for all of the mice to be examined in a single session. The software interface is designed for medical use and therefore retains clinical terminology (patient, doctor, exam) and data-handling strategies (first name, last name, and patient ID number are required entries; patients cannot be deleted once they are associated with data). These parameters must be adapted for mouse studies. Critically, the *New Patient* dialog box requires completing three fields (first name, last name, and ID number), and the ID number is limited by the software to ten characters. For simplicity, copy a unique sample identifier that includes the strain and mouse number, such as *JR0664_528*, into each field. Designation of left or right eye is added at each step of the acquisition (*see* **Note 12**).
3. Dilate the pupils of mice to be examined. Restrain and hold the mouse firmly in one hand, and squeeze a drop of dilating agent directly onto the surface of both eyes (or one eye, if only one will be examined). Allow 5–10 min for dilation to occur; the pupils will remain dilated for at least an hour. Whiskers (vibrissae) may be trimmed to prevent them from interfering with imaging, but with practice they may be displaced by the camera nosepiece, so this is unnecessary (*see* **Note 13**).
4. In the meantime, align the nodal point of the instrument with the metal phantom provided by the manufacturer.
5. Weigh mice that have been treated with dilating agent and record their weight. Anesthetize one mouse with the ketamine/xylazine cocktail, 0.10 mL/20 g body weight. The animal will become sedated with several minutes of injection. Assess anesthetization by the absence of movement when a hind paw is gently pinched.
6. Once the mouse appears sedated, apply a drop of GenTeal Severe gel to both eyes. This will prevent the corneal surface from drying prior to image acquisition.
7. Decide which eye will be imaged and orient the mouse stand (AIM-RAS in Bioptigen nomenclature) so that this eye is closest to the probe.
8. Apply Systane Ultra drops two to three times to wash away the GenTeal Severe gel from the eye being imaged, carefully removing excess liquid by touching a tissue to the corner of the eye while avoiding the corneal surface. Leave a small amount of liquid on the ocular surface to keep it moist during alignment of the eye with the optical path.

9. Place the mouse on the stand using the bite bar and dental cotton rolls or tissue on either side of the body to secure the mouse snugly within the stand. For small mice (10 g or less), additional padding may be required under the lower jaw to position the head and eye properly. Place the Velcro strap provided by the manufacturer over the back of the mouse to hold the mouse and padding in position.
10. Coarsely align the eye with the probe optical path. Place the red aiming tip on the end of the probe; if desired, it may be kept on continuously, although it may sometimes interfere with positioning. By turning the crank on the sample arm, advance the probe head to within several mm of the corneal surface. To move the mouse, twist the white cylindrical tube of the mouse stand and rotate the stand around the vertical axis until the eye is close to the center of the red aiming tip.
11. Initiate a live scan and make fine adjustments of the retinal image. Use the bite bar adjustment knobs and reference and sample arm positions until the optic nerve head is centered and the retinal layers and RPE are relatively free of curvature, horizontal in the left-hand live display, and vertical in the right. The choroid should be closest to the top of the left-hand live display. If necessary, the horizontal and vertical translation knobs on the mouse stand may be used for adjustment, but if they are used, the nodal point will be displaced, and may require recentering before the imaging the next mouse (*see* **Note 14**).
12. Once the eye is properly aligned, use a surgical spear to wipe away remaining eye drop liquid from the ocular surface to ensure a high-quality image (a slight realignment may be required if the eye is moved during this procedure) (*see* **Note 15**).
13. Acquire ten replicate scans in rapid succession. At a setting of $1000 \times 100 \times 1$, each scan takes ~3 s to acquire, and ~17 s to save (if only *.oct data are saved). If each scan is saved immediately following acquisition, a series of ten scans will require ~3 min (*see* **Note 16**).
14. If desired, rotate the mouse in the stand, align the remaining eye with the optical path, and image as described in **steps 10–13**.
15. Remove the mouse from the stand and repeat **steps 5–14** with the next mouse.
16. At the end of the session, transfer the OCT rectangular volume scans to a single folder. The software automatically saves several file types for each recording, but only *.oct files are needed for subsequent processing. Files are saved by default in a folder named *image* with the date as the folder name (*yyyy*.

mm.dd); the *.oct files can be sorted by type and copied to another folder or moved to a server.

17. Use the OCT Volume Averager plug-in in Fiji to register and average all scans from each session. The plug-in will automatically convert files from *.oct format to *.tif format, and perform registration and averaging functions on the *.tif formatted data. The output includes an image stack similar to the original volume and an orthogonal (*en face*) image stack that has been rescaled as needed to compensate for the unequal dimensions of nonisotropic scans. The performance of OCT Volume Averager is illustrated in Fig. 4. A B-scan from a single $1000 \times 100 \times 1 \times 1.4$ mm volume dataset is shown in Fig. 4a, and rescaled *en face* slices at different depths of the image stack are shown in Fig. 4c–f. The corresponding B-scan and *en face* views generated by OCT Volume Averager are shown in Fig. 4b and g–j, respectively. The use of the plug-in improves the signal-to-noise ratio, enhances the detection of detail in both B-scan and *en face* images, and reduces the horizontal banding that arises from eye movement due to the systemic pulse (*see* **Note 17**).
18. Image stacks generated by OCT Volume Averager may be manipulated in Fiji to review lesions and reveal morphological features of the posterior eye. One useful feature is the orthogonal displays generated by applying *Image> Stacks> Orthogonal Views* to *en face* datasets, which allow the user to assess where lesions or morphological features lie with respect to retinal layers, as shown Fig. 5a, b. A second useful feature is the *Image> Stacks> Tools> Grouped Z Project…*, which can project averaged subsets from the full *en face* volume based on user input, as shown in images of a wild-type C57BL/6J mouse shown in Fig. 5c. This approach allows assessment of tissue abnormalities at a glance. For example, dysplastic lesions in the inferior retina are readily identified in a homozygous *Crb1*^{rd8} mutant (compare Fig. 5d with c).

4 Notes

1. The Discover software allows files to be directly written in TIFF format, so additional time is not needed to convert to this format, as is the case in the Streampix software.
2. Fewer than 100 frames can be acquired to decrease raw data file size, but output should be assessed to ensure that image quality is acceptable. Acquisitions of >100 frames may be useful for additional downstream analysis.

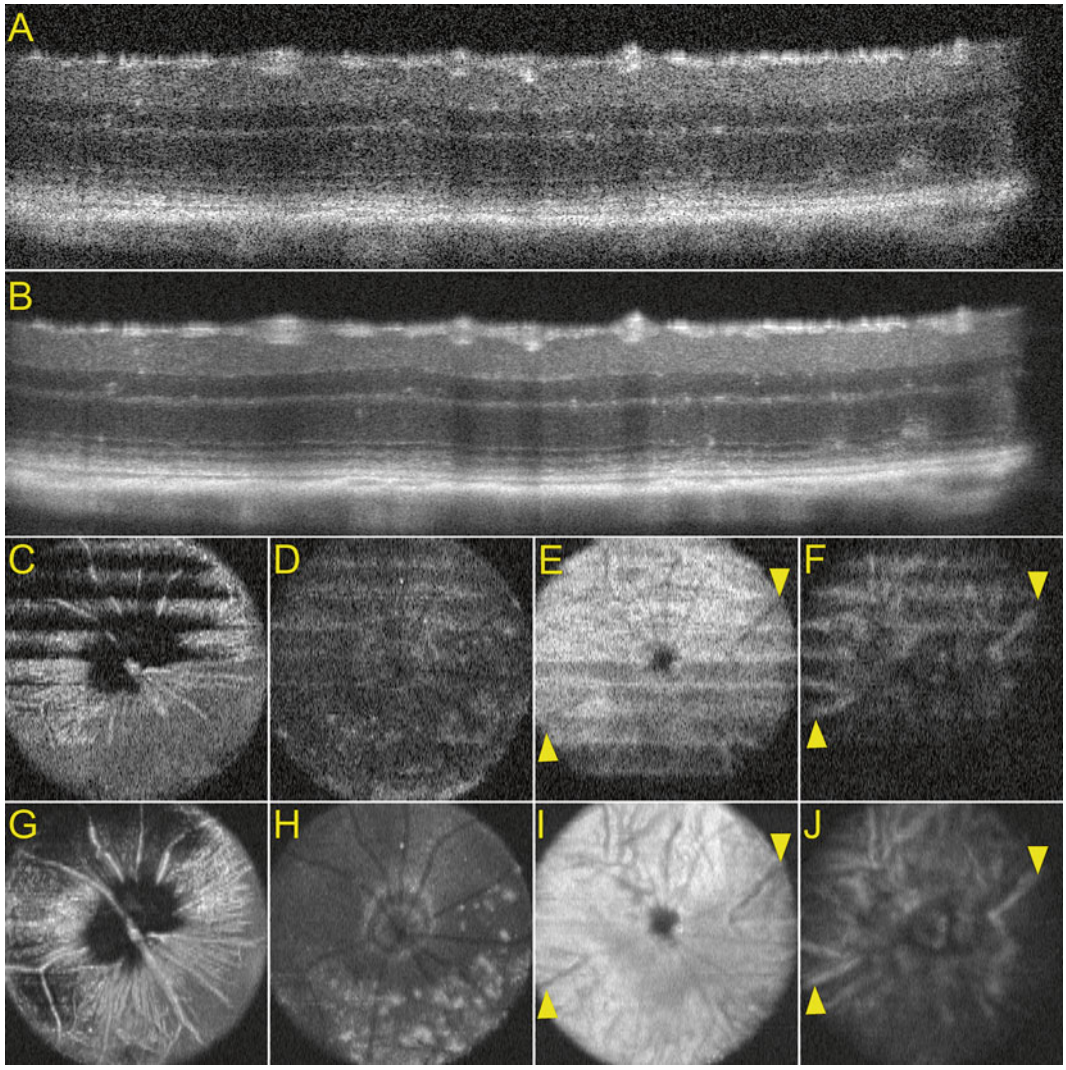

Fig. 4 OCT imaging. (**a**) B-scan from a single-volume dataset obtained from the right eye of a homozygous STOCK *Crb1*^{rd8} mouse (propagated and rederived from JAX Stock No. 003392). (**b**) B-scan at same position as in (**a**) obtained by registering and averaging 10 volumes with the OCT Volume Averager plug-in for Fiji. The processed image shows improved contrast and detection of detail. (**c**–**f**) Single *en face* images from a volume dataset at (**c**) the vitreoretinal surface, (**d**) the outer nuclear layer, (**e**) the choriocapillaris just beneath the RPE, and (**f**) the deeper choroid. Horizontal bands result from retinal movement during acquisition due to heartbeat and respiration. (**g**–**j**) Single *en face* images from the corresponding processed dataset. Details are enhanced and horizontal banding is substantially reduced. The large choroidal vessels near the optic nerve head in panels (**f**) and (**j**) (*arrowheads*), which are also evident as hyporeflective tracts in panels (**e**) and (**i**) (*arrowheads*), may correspond to the long posterior ciliary arteries and may be used to standardize ocular orientation

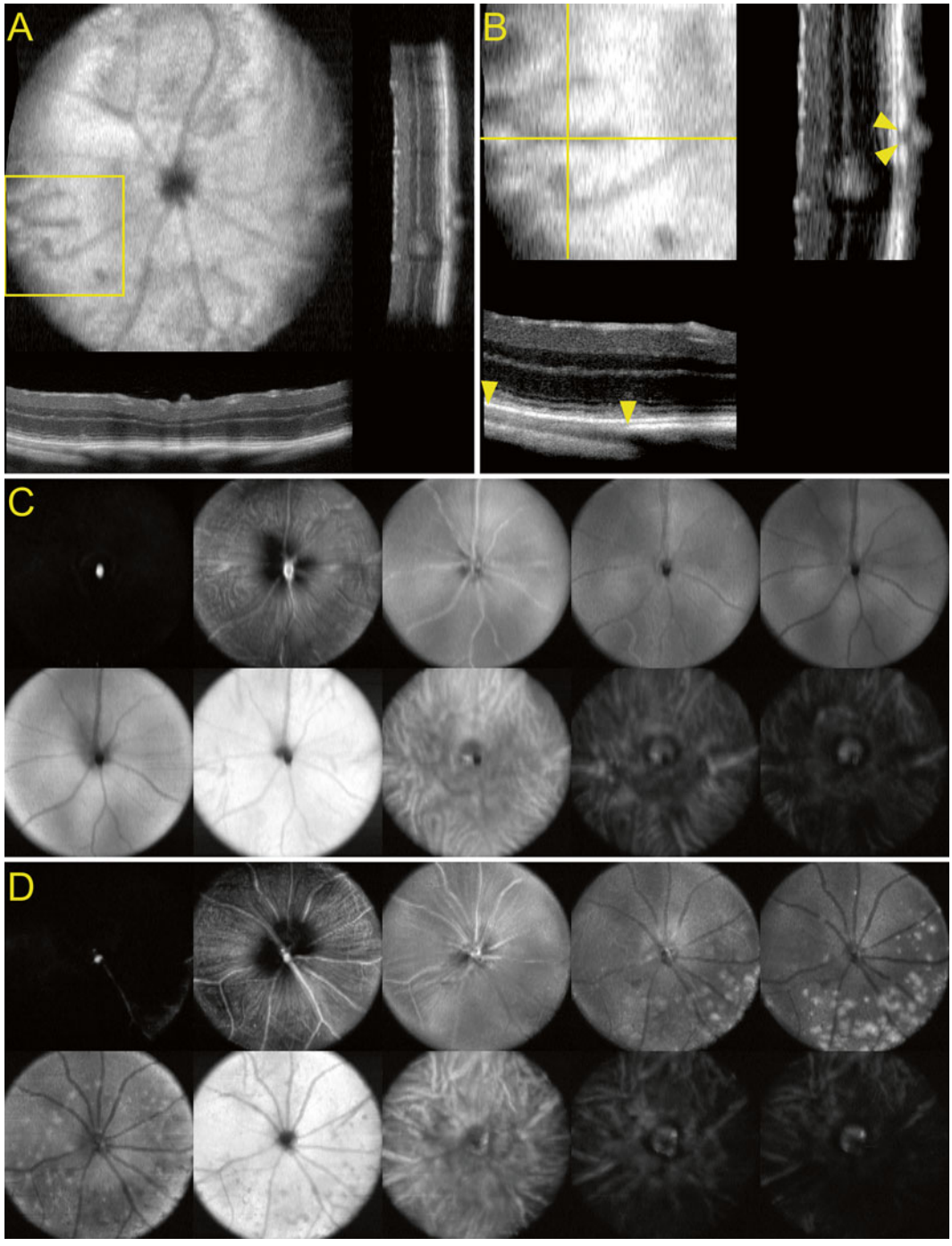

Fig. 5 Presentation of OCT imaging data in Fiji. (**a**) *En face* view of an OCT volume dataset of a mouse eye with orthogonal projections, useful for identifying the localization of lesions and vascular features with respect to retinal layers. In the image shown, the hyporeflective tracts observed at the level of the choroid in the *en face* view correspond to large-diameter tubelike structures in cross section, providing further evidence that these correspond to the long posterior ciliary arteries. (**b**) Detail of (**a**) showing the structure of the temporal long posterior ciliary artery near the optic nerve head. Note the gaps in the choroidal hyperreflective band between

3. The settings in **steps 1–4** will be retained when the program is launched subsequently, so they may be skipped after the program is first used.
4. To reduce the red appearance of the posterior eye in albino mice, the manufacturer recommends performing AWB with a pink card. This approach may also be used to manipulate the color balance of images acquired with the Micron IV camera, which has a sensor that yields images with a greater red contribution than those obtained with the Micron III instrument. A software feature that allowed users to adjust the gain of each channel independently might be the most desirable approach for manipulating color, to ensure the reproducibility of image parameters for downstream analysis. However, as of this writing, this approach is unavailable on the Micron systems.
5. Atropine may be toxic to the mouse if a large amount is accidentally ingested, so be sure to prevent drops from entering the mouth.
6. The mouse may be scruffed and mounted on the stand prior to applying GenTeal Severe gel. It is also possible to anesthetize the mouse prior to imaging, as described in **step 5** of the OCT acquisition and processing protocol. However, image contrast may be reduced in anesthetized animals due to modest opacification of ocular tissues.
7. This step is optional and should only be used if the rotational orientation of the eye is critical for downstream image analysis. Many mouse models of ocular disease, such as *Crb1*^{rd8} mice [22], show regional bias in the appearance or distribution of lesions in the retina and/or retinal pigment epithelium (RPE). Thus, methods to ensure a uniform ocular orientation may be essential for understanding pathogenic mechanisms.
8. In the Streampix software as originally provided by Phoenix Research Laboratories for a Micron IV installation at JAX,

Fig. 5 (continued) the *arrows*, which presumably correspond to areas where the artery displaces pigmented choroidal cells. (**c**) Grouped Z-projection showing features of the right eye of a C57BL/6J mouse (JAX Stock No. 000664) at different levels throughout the image. To generate a stack encompassing the tissue that could be divided into groups of manageable size (30 slices), the original *en face* image stack of 392 slices was cropped to 300 slices by *Image > Duplicate* with *Duplicate Stack* checked and a *Range* of 77–376. The *Projection Method* was then set to *Average Intensity* and *Group Size* was set to 30 for the *Grouped Z Project…* operation. The resulting stack was displayed with *Image > Stacks > Make Montage…* and *Image > Adjust > Brightness/Contrast… Auto* was used to optimize image appearance. This approach can be used to rapidly identify gross abnormalities in the posterior eye. (**d**) Grouped Z-projection of the homozygous *Crb1*^{rd8} eye shown in Fig. 4 with the same parameters as in (**c**). Note the abundant dysplastic lesions in the lower portion of the image, which corresponds to the inferior retina

exposure time was set to a default value of ~50 ms, the maximum allowed at a video acquisition rate of 20 frames per second (fps). Phoenix Research Laboratories provided greater flexibility in setting exposure times by upgrading their implementation of the Streampix software. Exposure time may be important for the highest quality images. In an unanesthetized mouse, the position of the retina may cycle 5–15 times per second due to the systemic pulse of ~300–900 beats/min, and the eye may undergo additional motion due to respiration at a rate of ~80–230 breaths/min [23]. Even under anesthesia, the heart rate is 300–450 beats/min and breathing is ~55–65 breaths/min [24]. Motional blurring and change in focus due to these physiological processes can be reduced by adjusting the exposure time to the minimum that allows sufficient image brightness. Exposure times of <20 ms are possible, but may result in dim images even if the source illumination is adjusted to its maximum. Gain may be increased to brighten the image, but this introduces noise that is undesirable for downstream processing. The Discover software does not currently allow adjustment of exposure time.

9. The Discover software includes an option to mark the image center onscreen.
10. The macro requires ~1–1.5 min to process a 100-slice TIFF file. The macro is available through the Fiji update site (http://fiji.sc/List_of_update_sites).
11. Bioptigen instruments on 32-bit Windows platforms can allocate sufficient memory to record at maximum a nonisotropic volume of 1000 A-scans per B-scan × 100 B-scans by 1 frame (abbreviated as 1000 × 100 × 1; frame refers to the number of repeat B-scans at the same raster position), or an isotropic volume of around 330 × 330 × 1. The nonisotropic approach allows high resolution in at least one dimension, and is therefore preferred for surveying fundus features, as in the protocol presented here. Newer Bioptigen 64-bit installations can acquire scans of 1000 × 1000 × 1; however, the resulting datasets appear to be too large for the capabilities of the Fiji OCT Volume Averager plug-in. Efforts are in progress to overcome this limitation. In the meantime, it is still possible to work with 1000 × 100 × 1 scans generated on these platforms, which can be exported in *.tif format by InVivoVue 2.2.20.
12. In more recent versions of the Bioptigen software, such as InVivoVue 2.2.20, more than ten characters may be used in the subject name. Nevertheless, the use of ten-character names should be retained, as the OCT Volume Averager plug-in is designed to recognize output from InVivoVue 1.4.0.4260.

13. Atropine may be toxic to the mouse if a large amount is accidentally ingested, so be sure to prevent drops from entering the mouth. If a mouse eye was treated with dilating agent earlier on the same day prior to OCT, an additional treatment may be unnecessary.
14. The procedure describes acquiring OCT data in enhanced depth imaging (EDI) mode, which emphasizes detail in the RPE and underlying choroid.
15. This is perhaps THE most important step to ensure high-quality images. Residual GenTeal Severe gel or drops can blur the OCT image considerably, so efficient removal of the liquid from the corneal surface is essential. The small amount of liquid that remains after the use of surgical spears appears to be sufficient to hydrate the eye during ten repeat rectangular volume scans.
16. Bioptigen InVivoVue 2.2.20 software on a 64-bit platform can acquire and save to disk in *.oct format the same total data volume in ~1.5 min (using a $1000 \times 100 \times 10$ scan), about half the time required by repeat scan protocol described here. Fewer keystrokes are required in the Bioptigen approach, as only one scan is initiated. Although both methods aim to produce an averaged rectangular volume with improved signal-to-noise, they differ in the acquisition schedule. In the approach presented here, the full image frame is acquired in one repeat. In the Bioptigen approach, ten repeats (frames) are obtained for each B-scan before moving to the next. Possible differences in the registered volume generated by these approaches have not yet been examined.
17. The OCT Volume Averager plug-in is available at the Fiji update site (http://fiji.sc/List_of_update_sites), and the corresponding source code at GitHub (github.com). The processing time for ten replicate rectangular volume scans ($1000 \times 100 \times 1$) using the OCT Volume Averager plug-in is ~20 min to create a *.tif image stack. By contrast, Bioptigen InVivoVue software 2.2.20 on a 64-bit platform can register and average a $1000 \times 100 \times 10$ scan and export the registered data in *.tif format in ~4.5 min. However, unlike OCT Volume Averager, the Bioptigen registration feature does not align adjacent slices of the averaged rectangular volume. In addition, the Bioptigen software cannot currently run in batch. Thus, additional hands-on time is required to load files from memory prior to registration and averaging, or to allow processing during the recording session.

References

1. Hawes NL, Smith RS, Chang B, Davisson M, Heckenlively JR, John SW (1999) Mouse fundus photography and angiography: a catalogue of normal and mutant phenotypes. Mol Vis 5:22
2. DiLoreto D, Grover DA, del Cerro C, del Cerro M (1994) A new procedure for fundus photography and fluorescein angiography in small laboratory animal eyes. Curr Eye Res 13:157–161
3. Nakamura A, Yokoyama T, Kodera S, Zhang D, Hirose S et al (1998) Ocular fundus lesions in systemic lupus erythematosus model mice. Jpn J Ophthalmol 42:345–351
4. Chang B (2013) Mouse models for studies of retinal degeneration and diseases. Methods Mol Biol 935:27–39. doi:10.1007/978-1-62703-080-9_2
5. Seeliger MW, Beck SC, Pereyra-Munoz N, Dangel S, Tsai JY, Luhmann UF, van de Pavert SA, Wijnholds J, Samardzija M, Wenzel A, Zrenner E, Narfstrom K, Fahl E, Tanimoto N, Acar N, Tonagel F (2005) In vivo confocal imaging of the retina in animal models using scanning laser ophthalmoscopy. Vision Res 45(28):3512–3519. doi:10.1016/j.visres.2005.08.014
6. Paques M, Simonutti M, Roux MJ, Picaud S, Levavasseur E, Bellman C, Sahel JA (2006) High resolution fundus imaging by confocal scanning laser ophthalmoscopy in the mouse. Vision Res 46(8–9):1336–1345. doi:10.1016/j.visres.2005.09.037
7. Srinivasan VJ, Ko TH, Wojtkowski M, Carvalho M, Clermont A, Bursell SE, Song QH, Lem J, Duker JS, Schuman JS, Fujimoto JG (2006) Noninvasive volumetric imaging and morphometry of the rodent retina with high-speed, ultrahigh-resolution optical coherence tomography. Invest Ophthalmol Vis Sci 47(12):5522–5528. doi:10.1167/iovs.06-0195
8. Fischer MD, Huber G, Beck SC, Tanimoto N, Muehlfriedel R, Fahl E, Grimm C, Wenzel A, Reme CE, van de Pavert SA, Wijnholds J, Pacal M, Bremner R, Seeliger MW (2009) Noninvasive, in vivo assessment of mouse retinal structure using optical coherence tomography. PLoS One 4(10):e7507. doi:10.1371/journal.pone.0007507
9. Alex AF, Heiduschka P, Eter N (2013) Retinal fundus imaging in mouse models of retinal diseases. Methods Mol Biol 935:41–67. doi:10.1007/978-1-62703-080-9_3
10. Schneider CA, Rasband WS, Eliceiri KW (2012) NIH Image to ImageJ: 25 years of image analysis. Nat Methods 9(7):671–675
11. Schindelin J, Rueden CT, Hiner MC, Eliceiri KW (2015) The ImageJ ecosystem: an open platform for biomedical image analysis. Mol Reprod Dev 82(7–8):518–529. doi:10.1002/mrd.22489
12. Schindelin J, Arganda-Carreras I, Frise E, Kaynig V, Longair M, Pietzsch T, Preibisch S, Rueden C, Saalfeld S, Schmid B, Tinevez JY, White DJ, Hartenstein V, Eliceiri K, Tomancak P, Cardona A (2012) Fiji: an open-source platform for biological-image analysis. Nat Methods 9(7):676–682. doi:10.1038/nmeth.2019
13. Low BE, Krebs MP, Joung JK, Tsai SQ, Nishina PM, Wiles MV (2014) Correction of the *Crb1*^{rd8} allele and retinal phenotype in C57BL/6N mice via TALEN-mediated homology-directed repair. Invest Ophthalmol Vis Sci 55(1):387–395. doi:10.1167/iovs.13-13278
14. Charette JR, Samuels IS, Yu M, Stone L, Hicks W, Shi LY, Krebs MP, Naggert JK, Nishina PM, Peachey NS (2016) A chemical mutagenesis screen identifies mouse models with ERG defects. Adv Exp Med Biol 854:177–183
15. Collin GB, Hubmacher D, Charette JR, Hicks WL, Stone L, Yu MZ, Naggert JK, Krebs MP, Peachey NS, Apte SS, Nishina PM (2015) Disruption of murine *Adamtsl4* results in lens zonular fiber detachment and retinal pigment epithelium dedifferentiation. Hum Mol Genet 24(24):6958–6974
16. Zhao LH, Spassieva S, Gable K, Gupta SD, Shi LY, Wang JP, Bielawski J, Hicks WL, Krebs MP, Naggert J, Hannun YA, Dunn TM, Nishina PM (2015) Elevation of 20-carbon long chain bases due to a mutation in serine palmitoyltransferase small subunit b results in neurodegeneration. Proc Natl Acad Sci U S A 112(42):12962–12967. doi:10.1073/pnas.1516733112
17. Saksens NT, Krebs MP, Schoenmaker-Koller FE, Hicks W, Yu M, Shi L, Rowe L, Collin GB, Charette JR, Letteboer SJ, Neveling K, van Moorsel TW, Abu-Ltaif S, De Baere E, Walraedt S, Banfi S, Simonelli F, Cremers FP, Boon CJ, Roepman R, Leroy BP, Peachey NS, Hoyng CB, Nishina PM, den Hollander AI (2016) Mutations in CTNNA1 cause butterfly-shaped pigment dystrophy and perturbed retinal pigment epithelium integrity. Nat Genet 48(2):144–151. doi:10.1038/ng.3474
18. Won J, Shi LY, Hicks W, Wang J, Hurd R, Naggert JK, Chang B, Nishina PM (2011) Mouse model resources for vision research. J Ophthalmol 2011:391384. doi:10.1155/2011/391384
19. Won J, Shi LY, Hicks W, Wang J, Naggert JK, Nishina PM (2012) Translational vision research models program. Adv Exp Med Biol 723:391–397.doi:10.1007/978-1-4614-0631-0_50

20. Li K (2008) The image stabilizer plugin for ImageJ. http://www.cs.cmu.edu/~kangli/code/Image_Stabilizer.html
21. Sedgewick J (2012) Scientific imaging: to sharpen or obscure? http://www.americanlaboratory.com/913-Technical-Articles/121695-Scientific-Imaging-To-Sharpen-or-Obscure/
22. Mehalow AK, Kameya S, Smith RS, Hawes NL, Denegre JM, Young JA, Bechtold L, Haider NB, Tepass U, Heckenlively JR, Chang B, Naggert JK, Nishina PM (2003) *CRB1* is essential for external limiting membrane integrity and photoreceptor morphogenesis in the mammalian retina. Hum Mol Genet 12(17):2179–2189. doi:10.1093/hmg/ddg232
23. Mouse Facts. http://www.informatics.jax.org/mgihome/other/mouse_facts1.shtml
24. Ewald AJ, Werb Z, Egeblad M (2011) Monitoring of vital signs for long-term survival of mice under anesthesia. Cold Spring Harb Protoc 2011(2):pdb prot5563. doi:10.1101/pdb.prot5563